Internal-tide generation and destruction by shoaling internal tides

S. M. Kelly[1] and J. D. Nash[1]

[1]   Internal-tide generation is usually predicted from local topography, surface tides, and stratification. However, internal tides are often observed to be unrelated to local spring-neap forcing, appearing intermittently in 3–5 day bursts. Here we suggest a source of this intermittency by illustrating how remotely-generated shoaling internal tides induce first-order changes in local internal-tide generation. Theory, numerical simulations, and observations show that pressure perturbations associated with shoaling internal tides can correlate with surface-tide velocities to generate or destroy internal tides. Where shoaling internal tides have random phase, such as on the New Jersey slope, time-averaged internal-tide generation is unaffected, but instantaneous internal-tide generation varies rapidly, altering internal-tide energy and possibly affecting nonlinear internal waves, across-shelf transport, and mixing. Where shoaling internal tides are phase-locked to the local surface tide, such as in double-ridge systems, time-averaged internal-tide generation is affected and may result in resonance. **Citation:** Kelly, S. M., and J. D. Nash (2010), Internal-tide generation and destruction by shoaling internal tides, *Geophys. Res. Lett.*, *37*, L23611, doi:10.1029/2010GL045598.

1.   Motivation

[2]   Internal (i.e., baroclinic) tides are generated where surface (i.e., barotropic) tides force stratified fluid to flow up and over sloping topography [*Garrett and Kunze*, 2007], extracting 0.7 ± 0.15 TW of energy from the surface tide [*Egbert and Ray*, 2000] and contributing to mixing that maintains the abyssal density distribution [*Munk and Wunsch*, 1998]. Along continental margins, internal tides drive sediment resuspension [*Butman et al.*, 2006], across-shelf transport [*Shroyer et al.*, 2010], and ecological processes [*Sharples et al.*, 2009].

[3]   Near major isolated topography such as the Hawaiian Ridge [*Rudnick et al.*, 2003], vertical heaving by the surface tide dominates the displacement of isopycnals, producing "coherent" internal tides that are phase-locked with local surface tides. Variability of internal-tide generation at such sites is largely explained by local spring-neap cycles in surface-tide forcing and changes in background stratification. Because these parameters are fairly predictable, previous studies have estimated global maps of quasi-steady internal-tide generation [e.g., *Nycander*, 2005]. These are supported by satellite observations, which resolve radiating internal tides that are coherent with the surface tide [*Ray and Mitchum*, 1996].

[4]   In-situ observations paint a different picture of the predictability of internal tides. These observations reveal that internal tides are intermittent and often uncorrelated with local spring-neap forcing [*Wunsch*, 1975]. Supporting evidence is common along continental margins, e.g., the California Bight [*Lerczak et al.*, 2003], Mozambique Channel [*Manders et al.*, 2004], North Carolina Shelf [*Savidge et al.*, 2007], Portuguese Shelf [*Sherwin et al.*, 2002], and Virginia Slope [*Nash et al.*, 2004].

[5]   Intermittent motions that are not phase-locked to the surface tide are termed "incoherent" [*van Haren*, 2004] and are spectrally manifested as a wide peak around the tidal frequency. Incoherence can arise as internal tides transit thousands of kilometers through mesoscale currents and stratification [*Zhao and Alford*, 2009], which alter their propagation speed and direction [*Rainville and Pinkel*, 2006], and cause their phase upon reaching distant locations to wander. Incoherence in observations of internal tides may therefore indicate the presence of remotely-generated internal tides.

[6]   Along continental margins, an idealized internal tide can be represented as a linear superposition of a locally-generated and remotely-generated shoaling internal tide:

$$u' = u'_{local} + u'_{shoal} \quad \text{and} \quad p' = p'_{local} + p'_{shoal}$$

where, u' and p' are internal-tide velocity and pressure (i.e., they have zero depth-average [*Kunze et al.*, 2002]). Conceptually, the locally-generated internal tide is forced by, and coherent with, the local surface tide, whereas the shoaling internal tide is forced by a remote surface tide, and may or may not be coherent with the local surface tide (Figure 1). In the following investigation, we examine the way in which shoaling internal tides impact internal-tide generation. We suggest that these dynamics explain some 3–5 day variability in internal-tide energy along continental margins.

2.   Decomposing Internal-Tide Generation

[7]   Internal-tide generation (sometimes referred to as topographic energy conversion) quantifies the rate of work per unit area on the internal tide by the surface tide. Over arbitrary topography, the linear limit for internal-tide generation is:

$$C = \nabla H \cdot \overline{\mathbf{U} p'}|_{z=H} \quad \left[\text{W/m}^2\right] \tag{1}$$

where $\mathbf{U}$ is surface-tide velocity, an overbar indicates a tidal average, $z = H$ defines the bottom, and ∇H is the topographic gradient [*Kurapov et al.*, 2003].

[8]   In this section we use four hydrodynamic simulations with idealized forcing to isolate internal-tide generation due to surface and shoaling-internal tides, i.e., $C = C_{local} + C_{shoal}$. Numerical simulations are conducted with the MIT

---

[1]College of Oceanic and Atmospheric Sciences, Oregon State University, Corvallis, Oregon, USA.
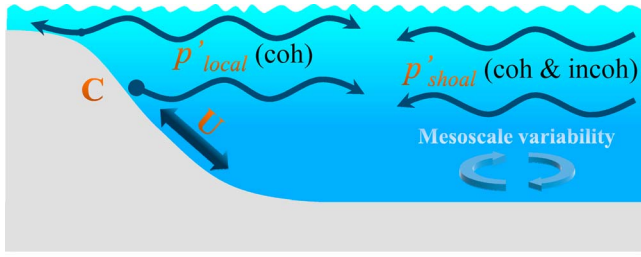
Figure 1. Internal tides on a continental slope. On the left, the surface tide **U** is deflected by the slope and produces pressure perturbations p'_{local} that are coherent with **U**. On the right, internal tides with pressure perturbation p'_{shoal} impinge on the slope. p'_{shoal} may, or may not, be coherent with **U**, as the propagating tides are scrambled by mesoscale features. Internal-tide generation C occurs along the sloping bottom and depends on how **U** covaries with p'_{local} and p'_{shoal}.

general circulation model [*Marshall et al.*, 1997] in a two-dimensional domain with 25-m horizontal and 5-m vertical resolution; planetary rotation is zero, buoyancy frequency is constant (ten times the semidiurnal frequency), and horizontal and vertical eddy viscosities are constant (10^{-1} and 10^{-2} m²/s, respectively). Semidiurnal forcing is applied at the boundaries and sponge conditions prevent reflection of outward-radiating internal tides. Continental-slope topography is half-Gaussian with a maximum slope that is supercritical with respect to a semi-diurnal internal-tide characteristic.

[9] When a surface tide is prescribed without a shoaling internal tide (BT sim.; Figures 2a, 2e, and 2i), all internal-tide pressure results from the displacement of isopycnals as

the surface tide encounters topography, i.e., $p' = p'_{local}$ (Figure 2a). Local internal-tide generation,

$$C_{local} = \nabla H \cdot \overline{\mathbf{U}p'_{local}}|_{z=H}, \qquad (2)$$

is positive (Figure 2i) and produces internal tides with energy fluxes ($F_E = \overline{u'p'}$ [*Kunze et al.*, 2002]) that radiate away from the slope (Figure 2e). C_{local} depends only on local topography, surface-tide forcing, and background stratification.

[10] In contrast, when a shoaling internal tide is prescribed without a surface tide (BC sim; Figures 2b, 2f, and 2j), internal-tide pressure is produced entirely by the shoaling internal tide, i.e., $p' = p'_{shoal}$ (Figure 2b). The resulting net internal-tide energy flux is onshore (Figure 2f) because the shoaling internal-tide is partially transmitted onto the continental shelf and partially reflected to the deep ocean. In this case,

$$C_{shoal} = \nabla H \cdot \overline{\mathbf{U}p'_{shoal}}|_{z=H} \qquad (3)$$

is approximately zero (Figure 2j), because $\mathbf{U} \approx 0$.

[11] In two cases that more closely resemble continental margins, surface and shoaling internal tides are prescribed simultaneously (BT+BC sims. 1 and 2). Internal-tide generation now contains contributions from both C_{local} and C_{shoal}. C_{local} is identical to the case with only surface tides. However, C_{shoal}, unlike the case with only shoaling internal tides, is no longer zero because $\mathbf{U} \neq 0$.

[12] In the presence of surface and shoaling internal tides C_{shoal} can be positive (BT+BC sim. 1; Figures 2c, 2g, and 2k) or negative (BT+BC sim. 2; Figures 2d, 2h, and 2l), depending on the phasing of surface tide velocity U and internal-tide bottom pressure $p'|_{z=H}$. When U and $p'|_{z=H}$ have
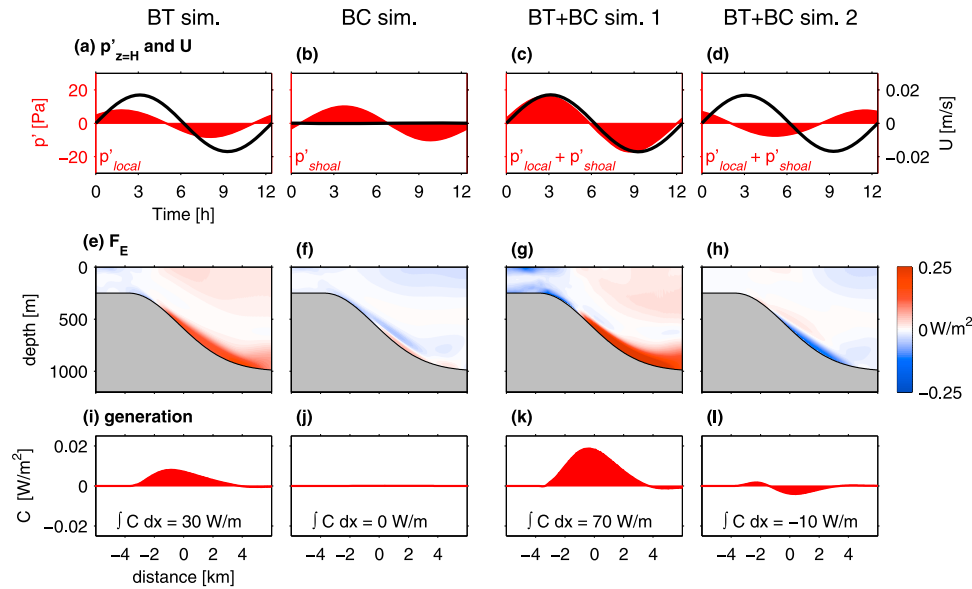
Figure 2. Four simulations of internal-tide generation. Columns from left to right: BT sim. is forced by a surface tide. BC sim. is forced by a shoaling mode-1 internal-tide. BT+BC sim. 1 is forced by surface and shoaling internal tides that are phased to maximize internal-tide generation. BT+BC sim. 2 is identical to BT+BC sim. 1, except the shoaling internal tide is phase shifted by 180° to minimize internal-tide generation. (a–d) Timeseries of internal-tide bottom pressure and surface-tide velocity at $x = 0$ km. The amplitudes and phasing of U and p' determines internal-tide generation. (e–h) Internal-tide energy flux. (i–l) Internal-tide generation and its horizontal integral.

positive covariance (BT+BC sim. 1; Figure 2c), the slope strongly radiates internal-tide energy (Figure 2g). In this case, $C_{shoal} > 0$, indicating additional energy is extracted from the surface tide (Figure 2k). Alternatively, when the phase of the shoaling internal tide is shifted by 180° (BT +BC sim. 2), U and $p'|_{z=H}$ have negative covariance (Figure 2d), and the slope weakly radiates internal-tide energy (Figure 2h). In this case, $C_{shoal} < 0$, indicating internal-tide energy is lost to the surface tide (Figure 2l), a process we term internal-tide destruction. *Kurapov et al.* [2003] identified $C < 0$ in numerical simulations and similarly associated it with remotely-generated internal tides. Internal-tide destruction is analogous to energy transfer from near-inertial waves to surface winds that oppose wave motion [*D'Asaro*, 1985].

[13] Thus, internal-tide generation depends on the phases and amplitudes of shoaling internal tides as well as local topography, surface tides, and stratification. Since shoaling internal tides depend on forcing at their origins, plus mesoscale variability (which influences their propagation), internal-tide generation is a global-scale phenomena. Furthermore, coupling between distant locations can occur because shoaling internal tides at one location are influenced by shoaling internal tides at their origins.

3. Incoherent Shoaling Internal Tides

[14] In the analysis of observations, it is often impossible to isolate p'_{shoal}. If it is assumed that shoaling internal tides have random phase, then p'_{shoal} can be estimated by identifying the component of p' that is incoherent with the local surface tide. This represents a lower bound on p'_{shoal} because an additional portion of the shoaling internal tide may be coherent with the local surface tide (Section 4).

[15] Here, we examine coherence in observations from the New Jersey slope [*Shroyer et al.*, 2010] to separate the locally-generated and shoaling internal tides. These observations were collected in the summer of 2006 from three moorings that recorded full-depth profiles of velocity and density. Coherent signals are extracted from band-passed records (which retain 4–30 hour variability) using least-squares harmonic regression to nine tidal frequencies. During the 40-day record, the coherent internal tide is modulated by the local spring-neap cycle and has divergent energy flux (Figures 3a and 3b). Conversely, the incoherent internal tide (computed as the difference between the band-passed and coherent timeseries) is intermittent, but contains no spring-neap variability and always produces onshore energy flux. We therefore associate coherent pressure and velocity with a locally-generated internal tide, and incoherent pressure and velocity with a shoaling internal tide.

[16] To illustrate the importance of the shoaling tide's phase, we examine C during a 7-day period in the middle of the record. During this period, p'_{local} is almost completely in phase with U (Figure 3c) so that C_{local} is maximized and varies slowly with the spring-neap cycle (Figure 3e, red). Conversely, p'_{shoal} drifts in and out of phase with U (Figure 3d) so that C_{shoal} varies on a 3–5 day timescale and is both positive and negative (Figure 3e, blue).

[17] Around 16 August, constructive phasing between p'_{shoal} and U (Figure 3d) produces a peak in total internal-tide generation (Figure 3e) that is not explained by local spring-neap forcing or background stratification. Three days

later, destructive phasing arrests internal-tide generation. These events are manifested in the record of internal-tide energy-flux divergence at the shelf break (Figure 3f), which is quantitatively consistent with internal-tide generation and destruction (Figure 3e), and indicates that the slope transitions from a 400 W/m source to a 200 W/m sink in just three days (Figures 3a and 3b). The timing of this transition, which occurs over a third of the spring-neap cycle, is dictated entirely by the phasing between p'_{shoal} and U.

[18] Because incoherent internal tides have random phase, they modulate instantaneous internal-tide generation, but do not affect its time average. While local models can estimate time-average C, they can not predict episodic bursts in C_{shoal} (and F_E), which may influence mixing, sediment resuspension, across-shelf transport, and other processes that are nonlinear functions of internal-tide energy.

4. Coherent Shoaling Internal Tides

[19] Shoaling internal tides can also be coherent with the local surface tide [*Colosi and Munk*, 2006]. When a shoaling internal tide is weakly affected by mesoscale variability, it arrives at the same phase each tidal period producing constant C_{shoal}. In double-ridge systems, such as within the Luzon Strait, internal-tide generation can be sensitive to topographic spacing and stratification [*Echeverri and Peacock*, 2010] because of coherent shoaling internal tides. Resonance occurs when time-averaged C_{shoal} is positive and the newly-generated internal tide propagates to the generation site of the original shoaling tide, producing positive C_{shoal} there and initiating an endless loop of intensification. For topographic features of limited spatial extent, resonance has been investigated using ray theory to identify internal-wave attractors [e.g., *Maas et al.*, 1997; *Tang and Peacock*, 2010]. Ray theory is less applicable to basin-scale topography where high-mode internal tides are rapidly attenuated.

[20] In addition, low-mode internal tides are observed to propagate thousands of kilometers, and their shoaling can induce the generation of subsequent low-mode internal tides. *Dushaw and Worcester* [1998] reported observations of a K1 internal tide resonating between Puerto Rico and the turning latitude, 1100 km to the North. They recognized an increase in internal-tide generation but did not propose a mechanism. We speculate that C_{shoal} was positive and increasing with each reflection.

5. Consequences

[21] Here we have shown that remotely-generated shoaling internal tides produce first-order changes in local internal-tide generation. The sign and magnitude of C_{shoal} depends on the correlation between surface-tide velocity and shoaling internal-tide pressure. Incoherent shoaling internal tides alter instantaneous internal-tide generation, while coherent shoaling internal tides alter time-averaged internal-tide generation.

[22] Historically, estimates of internal-tide generation have ignored shoaling internal tides by calculating generation completely from local forcing [e.g., *Nycander*, 2005]. Because these models can misrepresent time-averaged internal-tide generation (when internal tides are coherently shoaling), global models that include internal-tide propa-
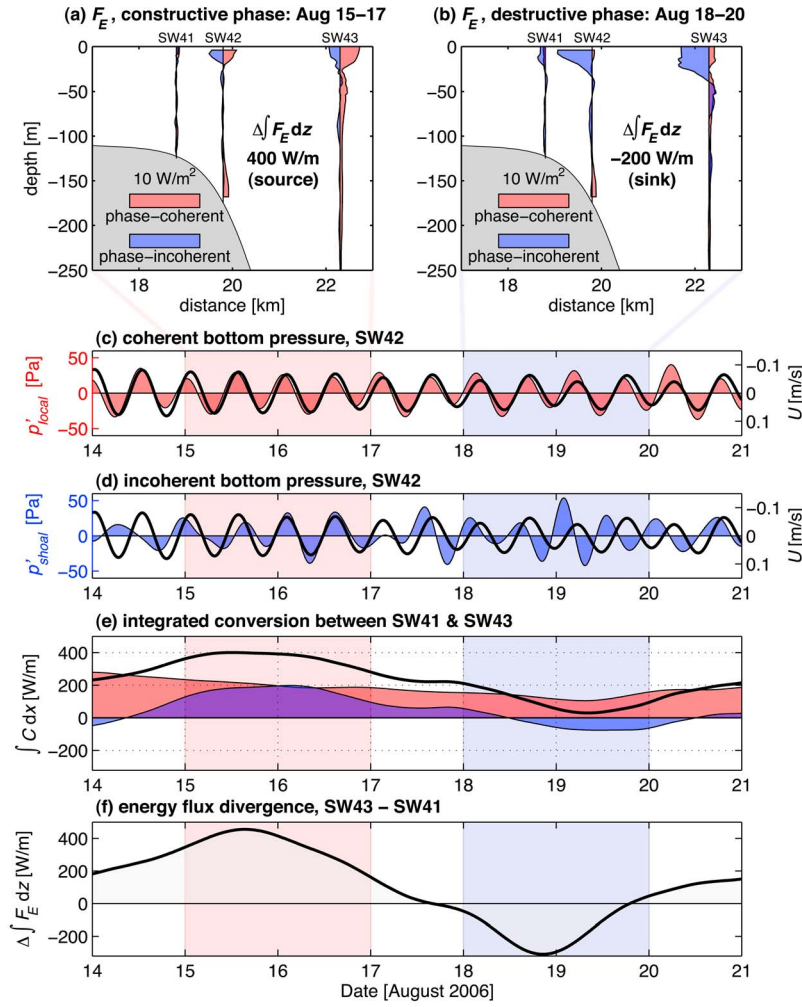
Figure 3. Observations from the New Jersey continental slope. (a and b) Coherent energy flux $\overline{u'_{local}p'_{local}}$ (red) is offshore, while incoherent energy flux $\overline{u'_{shoal}p'_{shoal}}$ (blue) is onshore. Total energy-flux divergence (which includes cross-terms) is indicated, and determines whether the slope is a source or sink of internal-tide energy. (c) p'_{local} (red) and **U** (black) are in phase throughout the record. (d) p'_{shoal} (blue) and **U** (black) drift in an out of phase. (e) As a result, integrated C_{local} (red) varies slowly in accordance with the local spring-neap cycle while C_{shoal} (blue) varies on a 3–5 day timescale. (e) Total internal-tide generation (black) and (f) energy-flux divergence (black) are quantitatively similar and significantly modified by C_{shoal}. Integrated C is are calculated from 2-km smoothed topography and the trapezoidal rule.

gation, dissipation, and shoaling [e.g., *Arbic et al.*, 2010] will eventually provide the best estimates of internal-tide generation. Unfortunately, global models with weakly damped internal tides may prove inherently chaotic because shoaling internal tides at one location are determined in part by shoaling internal tides at their places of origin. Until models with realistic internal-tide dissipation converge on a time-averaged map of internal-tide generation, satellite-derived estimates of surface-tide losses [*Egbert and Ray*, 2000] may provide the most reliable estimates of time-averaged internal-tide generation.

[23] More importantly, neither local nor global models can currently predict short-term variability in internal-tide generation. Episodic bursts in internal-tide energy and energy flux are likely to impact nonlinear mass, momentum, nutrient, and larval transports. In many locations, in-situ observations provide the only first-order accurate estimates of instantaneous internal tides.

References

Arbic, B. K., A. J. Wallcraft, and E. J. Metzger (2010), Concurrent simulation of the eddying general circulation and tides in a global ocean model, *Ocean Modell.*, *32*, 175–187.

Butman, B., P. S. Alexander, A. Scotti, R. C. Beardsley, and S. P. Anderson (2006), Large internal waves in Massachusetts Bay transport sediments offshore, *Cont. Shelf Res.*, *26*, 2029–2049.

Colosi, J. A., and W. Munk (2006), Tales of the venerable Honolulu tide gauge, *J. Phys. Oceanogr.*, *36*, 967–996.

D'Asaro, E. (1985), The energy flux from the wind to near-inertial motions in the surface mixed layer, *J. Phys. Oceanogr.*, *15*, 1043–1059.

Dushaw, B. D., and P. F. Worcester (1998), Resonant diurnal internal tides in the North Atlantic, *Geophys. Res. Lett.*, *25*, 2189–2192.

Echeverri, P., and T. Peacock (2010), Internal tide generation by arbitrary two-dimensional topography, *J. Fluid Mech.*, *649*, 247–266.

Egbert, G. D., and R. D. Ray (2000), Significant dissipation of tidal energy in the deep ocean inferred from satellite altimeter data, *Nature*, *405*, 775–778.

Garrett, C., and E. Kunze (2007), Internal tide generation in the deep ocean, *Annu. Rev. Fluid Mech.*, *39*, 57–87.

Kunze, E., L. K. Rosenfeld, G. S. Carter, and M. C. Gregg (2002), Internal waves in Monterey Submarine Canyon, *J. Phys. Oceanogr.*, *32*, 1890–1913.

Kurapov, A., G. Egbert, J. S. Allen, R. N. Miller, S. Y. Erofeeva, and P. M. Kosro (2003), The M_2 internal tide off Oregon: Inferences from data assimilation, *J. Phys. Oceanogr.*, *33*, 1733–1757.

Lerczak, J., C. Winant, and M. Hendershott (2003), Observations of the semidiurnal internal tide on the southern California slope and shelf, *J. Geophys. Res.*, *108*(C3), 3068, doi:10.1029/2001JC001128.

Maas, L. R. M., D. Benielli, J. Sommeria, and F. P. A. Lam (1997), Observation of an internal wave attractor in a confined, stably stratified fluid, *Nature*, *388*, 557–561.

Manders, A. M. M., L. R. M. Maas, and T. Gerkema (2004), Observations of internal tides in the Mozambique Channel, *J. Geophys. Res.*, *109*, C12034, doi:10.1029/2003JC002187.

Marshall, J., A. Adcroft, C. Hill, L. Perelman, and C. Heisey (1997), A finite-volume, incompressible Navier-Stokes model for studies of the ocean on parallel computers, *J. Geophys. Res.*, *102*, 5753–5766.

Munk, W., and C. Wunsch (1998), Abyssal recipes II: Energetics of tidal and wind mixing, *Deep Sea Res., Part I*, *45*, 1977–2010.

Nash, J. D., E. Kunze, J. M. Toole, and R. W. Schmitt (2004), Internal tide reflection and turbulent mixing on the continental slope, *J. Phys. Oceanogr.*, *34*, 1117–1134.

Nycander, J. (2005), Generation of internal waves in the deep ocean by tides, *J. Geophys. Res.*, *110*, C10028, doi:10.1029/2004JC002487.

Rainville, L., and R. Pinkel (2006), Propagation of low-mode internal waves through the ocean, *J. Phys. Oceanogr.*, *36*, 1220–1236.

Ray, R. D., and G. T. Mitchum (1996), Surface manifestation of internal tides generated near Hawaii, *Geophys. Res. Lett.*, *23*, 2101–2104.

Rudnick, D. L., et al. (2003), From tides to mixing along the Hawaiian Ridge, *Science*, *301*, 355–357.

Savidge, D. K., C. R. Edwards, and M. Santana (2007), Baroclinic effects and tides on the Cape Hatteras continental shelf, *J. Geophys. Res.*, *112*, C09016, doi:10.1029/2006JC003832.

Sharples, J., C. M. Moore, A. E. Hickman, P. M. Holligan, J. F. Tweddle, M. R. Palmer, and J. H. Simpson (2009), Internal tidal mixing as a control on continental margin ecosystems, *Geophys. Res. Lett.*, *36*, L23603, doi:10.1029/2009GL040683.

Sherwin, T. J., V. I. Vlasenko, N. Stashchuk, D. R. Jeans, and B. Jones (2002), Along-slope generation as an explanation for some unusually large internal tides, *Deep Sea Res., Part I*, *49*, 1787–1799.

Shroyer, E. L., J. N. Moum, and J. D. Nash (2010), Vertical heat flux and lateral mass transport in nonlinear internal waves, *Geophys. Res. Lett.*, *37*, L08601, doi:10.1029/2010GL042715.

Tang, W., and T. Peacock (2010), Lagrangian coherent structures and internal wave attractors, *Chaos*, *20*, 017508, doi:10.1063/1.3273054.

van Haren, H. (2004), Incoherent internal tidal currents in the deep ocean, *Ocean Dyn.*, *54*, 66–76.

Wunsch, C. (1975), Internal tides in the ocean, *Rev. Geophys.*, *13*, 167–182.

Zhao, Z., and M. H. Alford (2009), New altimetric estimates of mode-1 M_2 internal tides in the central North Pacific Ocean, *J. Phys. Oceanogr.*, *39*, 1669–1684.

─────────────

S. M. Kelly and J. D. Nash, College of Oceanic and Atmospheric Sciences, Oregon State University, 104 COAS Admin. Bldg., Corvallis, OR 97331, USA. (skelly@coas.oregonstate.edu)